applied sciences

MDPI

Article

Investigation on the Value-Added Production of Silicon Dioxide and Synthesizing Zeolites as well as Extraction of Rare Earth Elements from Fly Ash

Zhe Sun [1,2], Heyu Li [2,3,4], Zuimiao Tao [1,2], Baochuan Wang [5], Lei Gao [6], Yusheng Xu [6] and Yan Cao [1,2,3,4,5,*]

1 Anhui Province Key Laboratory of Chemistry for Inorganic/Organic Hybrid Functionalized Materials, Anhui University, Hefei 230601, China
2 Guangzhou Institute of Energy Conversion, Chinese Academy of Sciences, Guangzhou 510640, China
3 CAS Key Laboratory of Renewable Energy, Guangzhou 510640, China
4 Guangdong Provincial Key Laboratory of New and Renewable Energy Research and Development, Guangzhou 510640, China
5 Huainan Dongchen Group Co., Ltd., Huainan 232038, China
6 Shanxi Science and Technology Research Institute of Jinneng Holding Group, Taiyuan 030032, China
* Correspondence: caoyan@ms.giec.ac.cn

Abstract: Coal fly ash is one of the most promising secondary sources for extracting high value-added rare earth elements. Nevertheless, the majority of rare earth elements in coal fly ash are associated with the aluminosilicate glassy phase, hindering their solubility during the acid leaching process and resulting in the traditional rare earth elements extraction method, which is unavoidably complex in operation and poor in the economy. In this study, prior to the conventional acid leaching, the realization of the coal fly ash activation was considered. This consisted of two steps involving the coal fly ash calcination at the elevated temperatures using recyclable Na_2CO_3 and the water and alkali washing. It helped in developing the pore structures in coal fly ash, facilitating the leaching solution to rare earth elements, and reducing the acid consumption of rare earth elements leaching. Simultaneously, the generated aqueous solutions could precipitate two new valuable products, the purified silica oxide powder (257.58 $g \cdot kg^{-1}$, 338.1 $m^2 \cdot g^{-1}$ BET, 40 nm grain size, 93.43% purity) and porous zeolites (410.3 $g \cdot kg^{-1}$). The residual rare earth elements in the pretreated solid residue can be easily extracted, with an extraction efficiency of 91.24% and an acid saving rate of 74.5%. Therefore, a multiple of value-added products can be obtained by this new extraction method with great economic significance.

Keywords: CFA; rare earth elements; precipitated silica; zeolites; high value

check for updates

Citation: Sun, Z.; Li, H.; Tao, Z.; Wang, B.; Gao, L.; Xu, Y.; Cao, Y. Investigation on the Value-Added Production of Silicon Dioxide and Synthesizing Zeolites as well as Extraction of Rare Earth Elements from Fly Ash. *Appl. Sci.* **2023**, *13*, 7250. https://doi.org/10.3390/app13127250

Academic Editor: Dino Musmarra

Received: 11 May 2023
Revised: 9 June 2023
Accepted: 16 June 2023
Published: 17 June 2023

Copyright: © 2023 by the authors. Licensee MDPI, Basel, Switzerland. This article is an open access article distributed under the terms and conditions of the Creative Commons Attribution (CC BY) license (https://creativecommons.org/licenses/by/4.0/).

1. Introduction

The mining and use of coal resources over the years result in the great accumulation of coal-based solid wastes, which likely imposes threats to the environment and human society if they are not handled or used properly [1–3]. Coal fly ash (CFA) is one of representative coal-based solid wastes. Its current yearly production reaches more than 800 million tons worldwide, and more than 500 million tons [4,5] in China. To date, the CFA utilization in China has been hovering around 70%, and the reasonable and efficient utilization of CFA resources has become a critical issue. Previous great efforts have been made to apply CFA resources in construction, agriculture, and other fields, such as cement additives [6], brick and tile [7], ceramsite products [8], as well as for use in foundation and underground backfills [9]. Since the major compositions of CFA are SiO_2 and Al_2O_3 in a total of over 80%, they can be used as a suitable raw material to prepare a variety of silicon or aluminum-based products, such as silica, molecular sieve, silicon carbide, and glass ceramics [10–13].

The most recent effort has been made on the extraction of highly value-added REEs from CFA. Rare earth elements (including 15 lanthanides as well as yttrium and scandium

REEs) are an extremely important and critical strategic resource, widely used in various high-tech fields, such as national defense and military industry, aerospace, new energy, new materials, electronic information, etc. [14–16]. With the increasingly prominent contradiction between supply and demand, attention has been paid to prioritize the exploration of waste rich in REEs [17–20]. REEs are not particularly concentrated in coal, but CFA is enriched in REEs as a result of combustion [21]. Although REEs are still at their relatively low-occurring contents in CFA, the total amount of REEs reserve is still greater and attractable compared to the available REE ore resources due to the great quantity of CFA. Therefore, CFA can be regarded as an alternative source of REEs [22,23]. The successful and economic extraction of REEs from CFA can not only reduce the tension of the shortage of REEs, but also increase the value of CFA utilization.

The conventional method for extracting REEs is the enhanced acid or ammonia leaching [24–26]. This method requires highly corrosive solutions and is hazardous, energy intensive, and multistage. Owing to the presence of Al–Si-based glasses, the REEs extraction rate of this method is not sufficiently effective [27–29]. Meanwhile, this leaching method is indiscriminate, resulting in an impure mixture of REEs and bulk elements that require further separation processes [20]. Due to the dissolution of Si and the presence of sodium aluminate in the solution, the process of the desilication product (DSP) precipitation occurs. This leads to the high concentration of Na_2O (up to 14%), Al, and other impurities that precipitate along with the desilication product [30]. More importantly, this method functions efficiently on REEs in their ionic status, but fails in many cases of CFA-like raw materials, where the occurrence of REEs is in silicon–aluminum structures of CFA, in which acids or ammonia cannot be reachable. Currently, multiple parameters affecting the extraction of Al and Si from CFA have been analyzed in the published literature. Li et al. [31] studied the extraction of REEs from three primary phosphors by the high temperature alkali melting method, and investigated the effects of sodium hydroxide addition, calcination temperature, and calcination time on REEs leaching from phosphors. Ni et al. [32] investigated the effects of material addition ratio, alkali dissolution temperature, and time on REEs extraction in waste fluorescent powder. Huang et al. conducted extraction experiments on REEs in fly ash from a coal-fired power plant in China using 12 mol/L HCl or 16 mol/L HNO_3, and the leaching rate of rare earth elements was less than 20% [33]. Clearly, this will inevitably lead to an increase in the use of acid or ammonia during the leaching step and additional energy consumption by reactions between the CFA silicon–aluminum and leaching acids. Moreover, the neutralization step is generally necessary for the extraction process. Therefore, it is inevitably complex and inefficient in operation as well as poor in the economy. Consequently, stepwise desilication is significant in the synergistic utilization of CFA with the simultaneous extraction of Si, Al, and rare earth elements [34].

From the perspective of amplification of the extraction process, the collaborative utilization of various resources in CFA should be considered when researching and designing REEs extraction technology. For example, cement additives, building materials, and high value-added products, such as silica oxide powder and porous zeolite can be made based on their properties and composition characteristics during the REEs extraction process of CFA. In addition, the acid and alkali reagents consumed in the extraction process are the main source of cost, and it is necessary to consider the recycling of the extraction reagents.

Therefore, we proposed an improved process for REEs extraction, i.e., prior to the conventional acid leaching, a CFA activation was realized. This consisted of two steps: CFA calcination at elevated temperatures using Na_2CO_3 and water washing followed by alkali washing. This new additional procedure helped in the development of pore structures in CFA, the later-on access of leaching solution to REEs inside CFA, and the less acid consumption for the later-on REEs leaching. Simultaneously, the aforementioned water and alkali washing also generated aqueous solutions, leading to the generation of two new valuable products including the purified silica oxide powder and porous zeolites. The REEs in solid residue, which were generated from previous calcination and washing procedures, can be easily and successfully applied in a higher extraction efficiency via the

conventional leaching method in an acid saving manner. Meanwhile, the involved Na_2CO_3 can be recyclable. Moreover, a multiple of value-added products can be obtained by this new extraction method with great economic significance.

In this study, various process parameters (i.e., NaOH concentration, heating temperature, solid–liquid ratio, and holding time) will be investigated and optimized to maximize the silicon and aluminum recovery through alkali leaching of the activated CFA sample. Additionally, the obtained value-added products will be evaluated, and the effect of water and alkali washing operation on REEs extraction efficiency as well as acid saving rate will be investigated, in order to achieve the process coupling of REEs extraction process and effective utilization of all substances in CFA.

2. Materials and Method

2.1. Materials

The CFA sample was obtained from a coal-fired power plant in Anhui Province, China. The main elements of CFA sample were analyzed using XRF (X-ray Fluorescence Spectrometer) (ZSX-Primus, Tokyo, Japan), and the results are shown in Table 1. The highest contents in the CFA sample are Si and Al, as well as some Fe and Ca.

Table 1. XRF analysis of a power plant sample in CFA.

Element	Si	Al	Fe	Ca	Na	K	Mg	O	Other
Content/%	26.08	14.66	2.04	0.63	0.49	1.02	0.24	44.43	10.41

The analysis of REEs in the CFA sample was conducted by digestion in a microwave digester and tested using ICP-MS (Inductively coupled plasma-Mass Spectrometry) (ICAP-Q, Waltham, MA, USA). REE contents of the CFA sample were shown in Figure 1. The average content of total REEs reaches 455 ppm ($mg \cdot kg^{-1}$), with a standard deviation of 4.4 ppm. The major REEs in CFA were found to be the light REEs (LREEs), such as La, Ce, and Nd. The average content of total heavy REEs (HREEs) is about 132 ppm (standard deviation is 1.5 ppm), among them, Sc and Y account for the highest. The ratio of heavy and light REEs was 2:5.

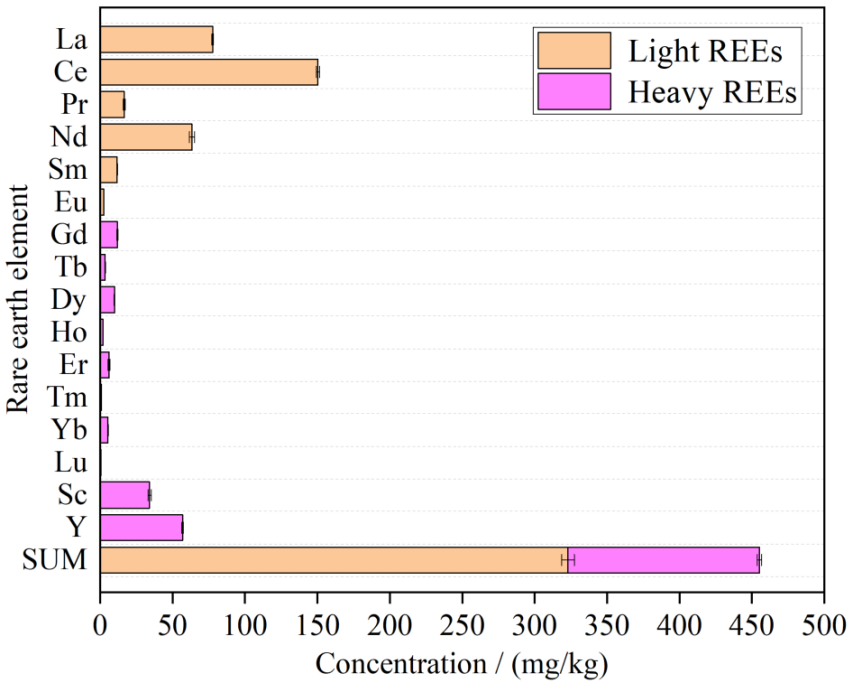


Figure 1. Content of REEs in CFA sample activation.

The reagents required for the experiment, including Na_2CO_3, NaOH, and HCl, were all of analytical grade from Sinopharm Chemical Reagent Co., Ltd., Shanghai, China, the deionized water was of EW—I purity from Shandong Youwei Chemical Co., Ltd., Jinan, China, and the CO_2 (≥99.999%) was from Dalian Special Gases Co., Ltd., Dalian, China.

2.2. Experiment

The experiment was conducted following five steps: Activation, extraction of silicon and aluminum, synthesis of precipitated silica, synthesis of zeolites, and REEs leaching. Parallel experiments were conducted to ensure the reproducibility of the results. Figure 2 shows the experimental scheme, and the detailed procedures were given as follows:

a. Sample activation: First, 1 g of the CFA sample was quantitatively weighed. The alkali additive of Na_2CO_3 was weighed and mixed with the CFA sample at a molar ratio of 1:1 (the ratio of silicon and aluminum content to the additive). The mixtures were calcinated in a muffle furnace to a certain temperature of 850 °C and maintained for a desirable time of 80 min. Then, the sample was cooled to an ambient temperature and ground in agate mortar for the subsequent procedures.
b. Leaching of silicon and aluminum: The activated sample was transferred to a beaker and stirred with 20 mL of deionized water at an ambient temperature for 30 min. The solid–liquid separation was performed and repeated three times. To maximize the silicon and aluminum recovery through alkali leaching of the activated CFA sample, the process was optimized for the process parameters, i.e., NaOH concentration, heating temperature, solid–liquid ratio, and holding time. The desired concentration of the NaOH solution and other factors was based on the orthogonal table (Table 2). The washed samples were transferred to a round-bottom flask, and the bottle mouth was tightened with a rubber plug. The round-bottom flask was placed in an oil bath at a set temperature by magnetic stirring. The sample was centrifuged to separate the solid–liquid phase after the reaction. Leaching solution after water and alkali washing and separation was subject to the determination of Si and Al using ICP-OES (Inductively Coupled Plasma Optical Emission Spectrometer) (ICAP 7400, Waltham, MA, USA).
c. Synthesis of precipitated silica: The water washing solution of the activated CFA sample was collected and transferred to a beaker. CO_2 gas was introduced at a controlled flow rate and the pH was monitored until the solution pH stabilized at about 8.00. The solution was then transferred to the centrifugal tube and aged for 24 h at an ambient temperature. Thereafter, the solid-phase sample was separated and washed with deionized water several times and finally dried at 100 °C to obtain the precipitated silica product.
d. Synthesis of zeolites: The solution obtained during the alkali leaching experiment was used as the mother liquor for the synthesis of zeolite via the hydrothermal crystallization method [35]. The solution was stored at an ambient temperature for 24 h, and the precipitation of an orange-yellow solid in the solution was observed. The solid–liquid mixtures were transferred to the crystallization kettle and crystallized at 100 °C for 1, 3 and 5 h, and then followed by the separation of the solid-phase sample and washed with deionized water several times. Finally, the solid sample was dried in the oven at 100 °C to obtain zeolite products, and the separated liquid-phase sample can be used as a fresh alkali washing solution for activated CFA samples.
e. Leaching of REEs: The solid sample residue after the aforementioned activation and washing procedure was respectively added into 20 mL of deionized water and stirred evenly in a constant ambient temperature using a magnetic stirrer. A certain volume of concentrated hydrochloric acid was gradually added with a pipette gun to maintain the solution pH at 2.00. Finally, the liquid-phase sample was separated and subject to the determination of REEs using ICP-MS (ICAP-Q, Waltham, MA, USA).

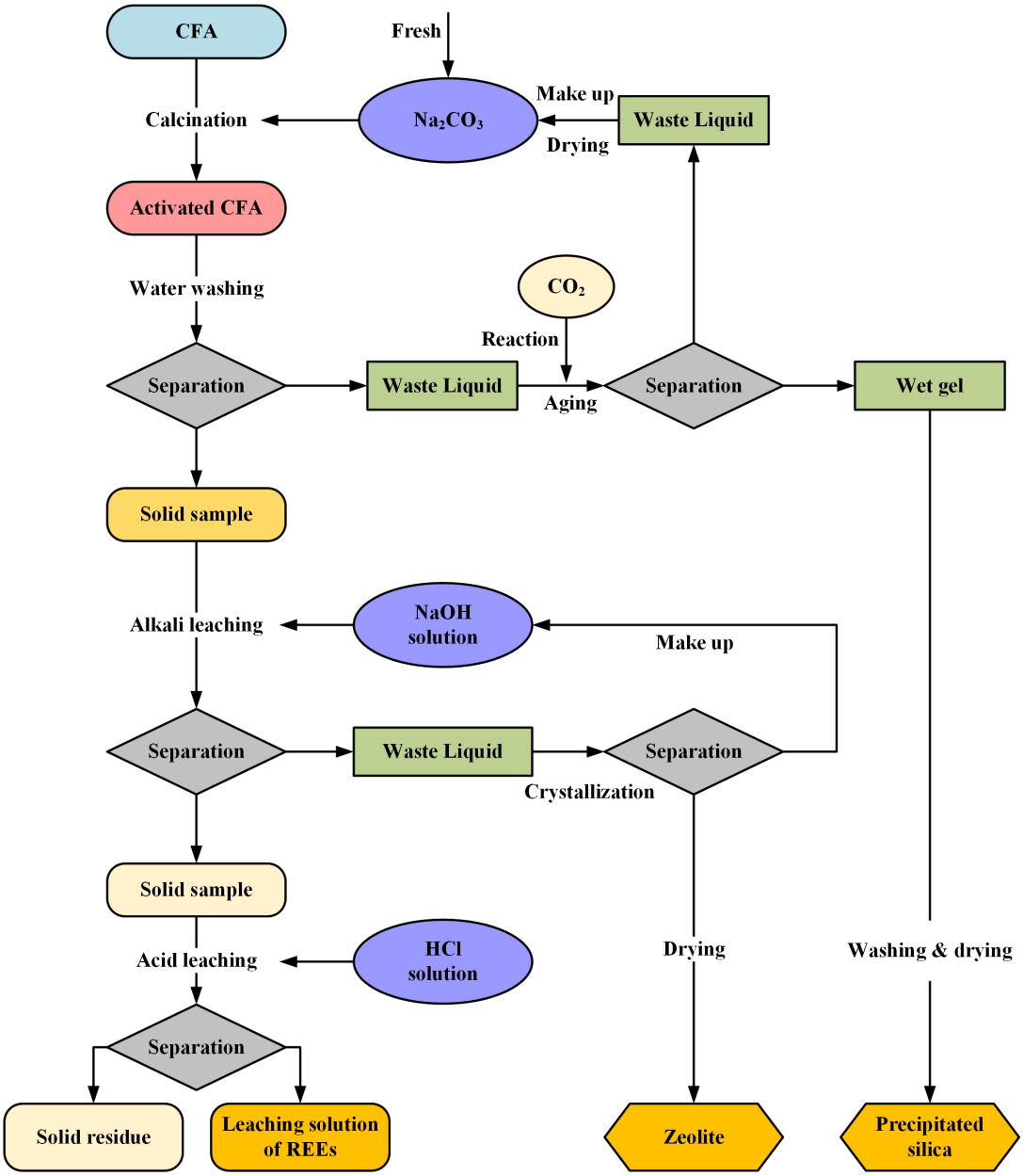


Figure 2. The design of experimental scheme.

Table 2. Orthogonal experimental table of alkali leaching of CFA-activated sample.

Level \ Factor	Concentration (A)/%	Temperature (B)/°C	Solid–Liquid Ratio (C)	Time (D)/h
1	10	60	1:10	0.5
2	15	75	1:15	1
3	20	90	1:20	1.5

For the characterization of value-added solid products, the crystalline phase evolution of zeolites was analyzed by XRD (SmartLab, Tokyo, Japan) with Cu Kα radiation (40 kV, 40 mA) at a scan rate of 2°/min and step size of 0.0167°. The micromorphology of the silica product and zeolites was performed by SEM (Hitachi S4800, Tokyo, Japan) and TEM (JEM-2100, Tokyo, Japan). In addition, the pore characteristics were determined by BET (ASAP 2460, Shanghai, China).

3. Results and Discussion

3.1. Extraction of Silicon and Aluminum in CFA

After the sample was calcinated with Na_2CO_3, the original silicate aluminate and glass phase structure in CFA could be destroyed, and new silicate or silicate aluminate structures with high activity were likely generated. This activated CFA sample mainly contains a large amount of insoluble aluminosilicate, some water-soluble Na_2SiO_3, and a small amount of $NaAlO_2$. The specific experimental reactions were likely as follows:

$$Al_6[SiO_4]_2O_5 + 4SiO_2 + 3Na_2CO_3 \rightarrow 6NaAlSiO_4 + 3CO_2\uparrow \quad (1)$$

$$Al_2O_3 + Na_2CO_3 \rightarrow 2NaAlO_2 + CO_2\uparrow \quad (2)$$

$$SiO_2 + Na_2CO_3 \rightarrow Na_2SiO_3 + 2CO_2\uparrow \quad (3)$$

Among them, the majority of Na_2SiO_3 and a small amount of $NaAlO_2$ can be easily removed with simple water washing. The remaining solution is mostly insoluble silicate aluminate, which was likely continuously washed-out using an alkaline solution. The alkaline solution can easily decompose the silicate aluminate into soluble aluminate and silicate, in order to achieve the extraction of silicate aluminate, following a reversible reaction of the alkali dissolution process as follows:

$$\text{Aluminosilicate (solid phase)} \rightleftharpoons \text{Aluminate ion (liquid phase)} + \text{Silicate ion (liquid phase)} \quad (4)$$

Experimental results showed that the water-washed CFA achieved the Si extraction efficiency of 51.46% and Al of only 2.07%. The alkali washing treatment was carried out after the orthogonal experiment as shown in Table 3. It was found that the extraction efficiency of Si and Al elements changed significantly under different levels of factors. The range R helped in judging the influence degree of each factor in the experiment, showing that the significance of factors followed the sequence of the solid–liquid ratio (C), the NaOH concentration (A), the holding time (D), and the heating temperature (B). The k-value was calculated according to the extraction efficiency of the Al element in each group. The effect curves of each factor were drawn leading to the optimal combination of conditions, in order to achieve the maximum extraction of Al. When the NaOH concentration is 20% (A3), the heating temperature is 60 °C (B1), the solid–liquid ratio is 1:20 (C3), and the holding time is 1 h (D2), then the extraction efficiency of Al and Si can be achieved by 62.51% and 36.82%, respectively.

Table 3. Alkali leaching orthogonal experiment.

Group	Factor				Al Dissolution Rate	Si Dissolution Rate
	A	B	C	D		
1	0.1	60	1:10	0.5	14.91%	7.26%
2	0.1	75	1:10	1	24.24%	12.65%
3	0.1	90	1:10	1.5	29.59%	14.23%
4	0.15	60	1:15	1.5	33.02%	17.72%
5	0.15	75	1:15	0.5	39.73%	27.10%
6	0.15	90	1:15	1	27.68%	11.24%
7	0.2	60	1:20	1	62.51%	36.82%
8	0.2	75	1:20	1.5	14.87%	7.81%
9	0.2	90	1:20	0.5	42.42%	25.05%
K1	22.91%	36.81%	19.15%	32.35%		
K2	33.48%	26.28%	33.23%	38.14%		
K3	39.93%	33.23%	43.94%	25.83%		
R	17.02%	3.59%	24.79%	6.52%		
Best combination	A3	B1	C3	D2	62.51%	36.82%

3.2. Precipitation of Silica

The synthesis method of silica powder followed the chemical precipitation method introduced in Refs. [36–38]. Generally, the precipitation uses the strong acid (H_2SO_4, HCl) as a precipitant to move the Na_2SiO_3 reaction in the solution. Alternatively, in this study, the carbonation method [39] was used for the silica precipitation, where CO_2 gas was introduced into the water washing solution from the activated CFA sample containing sodium silicate. The switch of precipitant made the process cheaper, less corrosive, and recoverable in the calcination of Na_2CO_3. The experimental reaction is shown as follows:

$$Na_2SiO_3 \cdot nH_2O + CO_2Na_2CO_3 + SiO_2 \cdot nH_2O\downarrow \quad (5)$$

The average yield of precipitated silica products prepared in the experiment was approximately 257.58 $g \cdot kg^{-1}$. Figure 3 shows the TEM image of the silica product obtained. It is found that a certain degree of agglomeration occurred in the silica product with its size smaller than 0.5 μm, while the size of the single SiO_2 particle can be as small as 40 nm, implying the nanometer level of the precipitated silica.

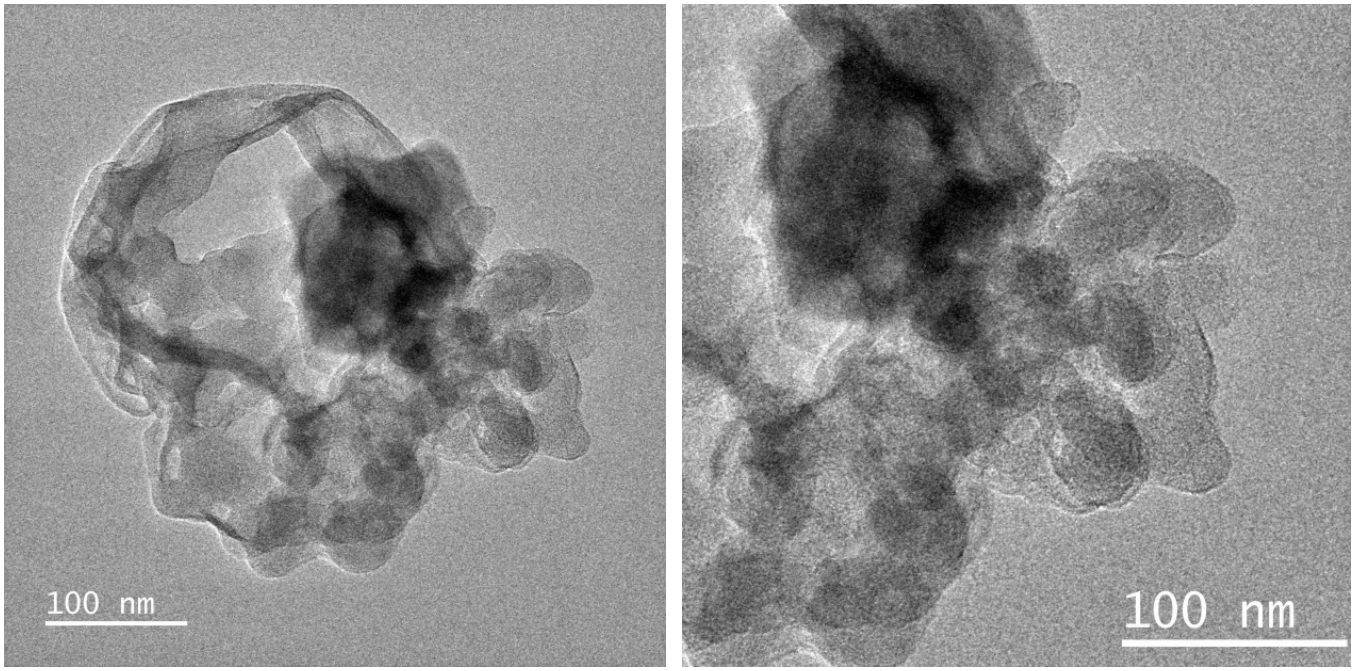


Figure 3. TEM diagram of precipitated silica synthesized by the carbonation method.

The purity analysis of silica products in parallel experiments using the XRF analysis was shown in Table 4, indicating that the average content of SiO_2 in the product reached 93.43%. The trace elements of Cu, Fe, and Mn were within the allowable range, implying that its quality conforms with the Standard HG/T 3061-2009. As a value-added byproduct, the size of nanoscale silica is crucial when extracting rare earth elements. The smaller the particle size of nanoscale silicon dioxide, the larger its specific surface area, the larger its surface energy, the higher its dispersity, and the stronger its adsorption capacity and reinforcing property. The precipitated nano-silica powder in this study was found to be loose in packing, white in color, and good in dispersibility. By weighing the material and energy costs of the whole process, the BET analysis showed that its specific surface area can be achieved by 338.0512 $m^2 \cdot g^{-1}$, which belongs to the class A (>191 $m^2 \cdot g^{-1}$) commercial white carbon black single crystal.

Table 4. Performance test of precipitated silica.

Component	Content	HG/T 3061-2009	Result
SiO_2 content	93.43%	≥90%	Qualified
Heating reduction	5.33%	4.0–8.0%	Qualified
Ignition reduction	6.67%	<7.0%	Qualified
Fe content	0.034%	≤0.05%	Qualified
Mn content	0.0029%	≤0.004%	Qualified
Cu content	0.0008%	≤0.001%	Qualified

3.3. Synthesis of Zeolites

Figure 4 shows the XRD images of the solid substances which were crystallized from the alkali washing solution of the activated CFA sample naturally settled at an ambient temperature of (0 h), and then for 1, 3, and 5 h. By comparing the XRD images of zeolites at different crystallization times in the parallel experiment, although the peak intensities of the two groups of experiments were slightly different, the coexistence of NaA and sodalite zeolites as well as the mechanism from NaA zeolite to sodalite zeolite during the phase-transformation process can be clearly manifested. The XRD spectra for 0 h clearly indicated a small characteristic peak of NaA zeolite in addition to a large bulge corresponding to the most-amorphous solid phase. Greer et al. [40] investigated the early reverse crystal growth of zeolite A and its phase transition to sodalite, and found that in the early phase transition stage, crystallization will occur on the surface of amorphous spherical particles formed by precursors and polymers, forming a typical cubic morphology related to zeolite A. It has a very thin crystalline cubic shell and amorphous core. When the solution was crystallized at 100 °C, the amorphous material started to transit toward the structure of NaA zeolite. This was clearly shown in its XRD spectrum of the sharp and narrow characteristic peak of NaA zeolite after 1 h of crystallization. With the extension of crystallization from surface to core, sodalite zeolite nanoplates were crystallized within the amorphous nucleation of these NaA zeolite cubes. As validated in Figure 4, the crystallization time was extended to 3 h and reversely weakened the intensity of the NaA characteristic peak; however, it strengthened a new characteristic peak corresponding to the sodalite zeolite. This was likely due to the fact that OH^- was produced during the formation of NaA crystal form, resulting in an increase in alkalinity of the solution system. The environment with higher alkalinity was more conducive to the nucleation of sodalite zeolite. In addition, the skeleton energy of NaA structure was higher than sodalite, leading to a trend of spontaneous transformation toward sodalite [22]. As expected, the extension of the crystallization time to 5 h completely transformed the NaA zeolite to be the sodalite zeolite, as evidenced by the only narrow and sharp sodalite characteristic peaks that remained in spectrum of the obtained zeolite product. Combined with the research of Subotic et al. [41], the phase transformation of NaA zeolite to sodalite zeolite mainly includes the following steps: Dissolution of NaA zeolite particles, supersaturation of liquid phase and aluminosilicate ions, and nucleation of hydroxy sodalite from the solution and crystal growth of sodalite. Meanwhile, the D-spacing in Table 5 showed an increasing trend with the crystallization time, indicating that the atomic arrangement of the synthesized zeolite was more compact.

Figure 5 shows the SEM images of the zeolite crystallized from the alkali washing solution of the activated CFA sample for 1, 3, and 5 h, and then naturally settled at an ambient temperature. It indicated the variation of morphologies of zeolite by controlling the crystallization reaction time. It shows spherical aggregates of amorphous silicate aluminate particles in small particle sizes with only a very small amount in the NaA zeolite structure. After crystallization for 1 h at the elevated temperature, the spherical particles in the solid phase disappeared and cubic grains of complete NaA zeolite clearly appeared [23], showing the "stacking" growth phenomenon. After crystallization for 3 h, only a small part of regular crystal shape NaA grains was found in the solid phase, in contrast to the majority in sodalite structure with an irregular shape, chimeric with each other, and in flower cluster. The SEM image further revealed that sodalite grains considered the surface of NaA crystal

as its heterogeneous crystallization center, nucleated on the surface of NaA crystal, and developed into cluster-shaped aggregates. This was due to the fact that polar solvent ions were easily adsorbed on the grain surface in the alkaline hydrothermal system [24], and the growth into aggregate could overcome the nucleation barrier. When the crystallization time was further extended to 5 h, the complete disappearance of the NaA zeolite and the whole formation of sodalite occurred, showing the spherical shape as a whole which was agreeable with the literature description [25]. Therefore, both XRD and SEM analyses evidenced that the increased crystallization time at an elevated temperature accelerated the structure changes from NaA toward sodalite. The longer the time, the more sodalite is present in the zeolite products. The crystallization time of 5 h significantly increased the zeolite yield to be as high as 410.3 $g \cdot kg^{-1}$.

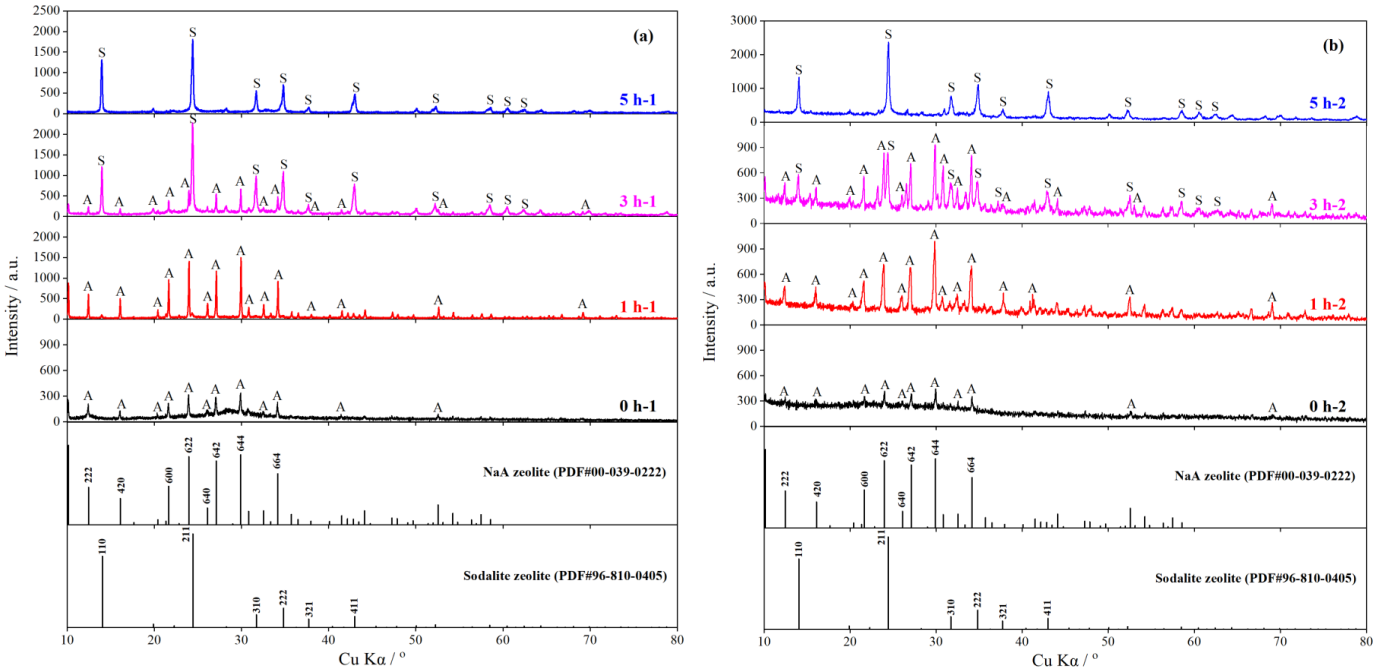


Figure 4. XRD images of zeolites synthesized at different crystallization times. (**a**,**b**) The sample XRD results of two parallel experiments, respectively (S—sodalite zeolite; A—NaA zeolite).

Table 5. D-spacing of zeolites synthesized at different crystallization times (based on XRD results).

Crystalline	Crystal Face (d/nm)	Sample							
		0 h	0 h—2	1 h	1 h—2	3 h	3 h—2	5 h	5 h—2
NaA zeolite	622	0.7411	0.7406	0.7413	0.7417	0.7422	0.7431	-	-
	642	0.6573	0.6574	0.6585	0.6576	0.6606	0.6594	-	-
	644	0.5964	0.5966	0.5970	0.5968	0.5986	0.5979	-	-
	664	0.5242	0.5242	0.5248	0.5245	0.5255	0.5252	-	-
Sodalite zeolite	110	-	-	-	-	1.2657	1.2655	1.2659	1.2660
	211	-	-	-	-	0.7286	0.7284	0.7290	0.7294
	222	-	-	-	-	0.5152	0.5146	0.5153	0.5158

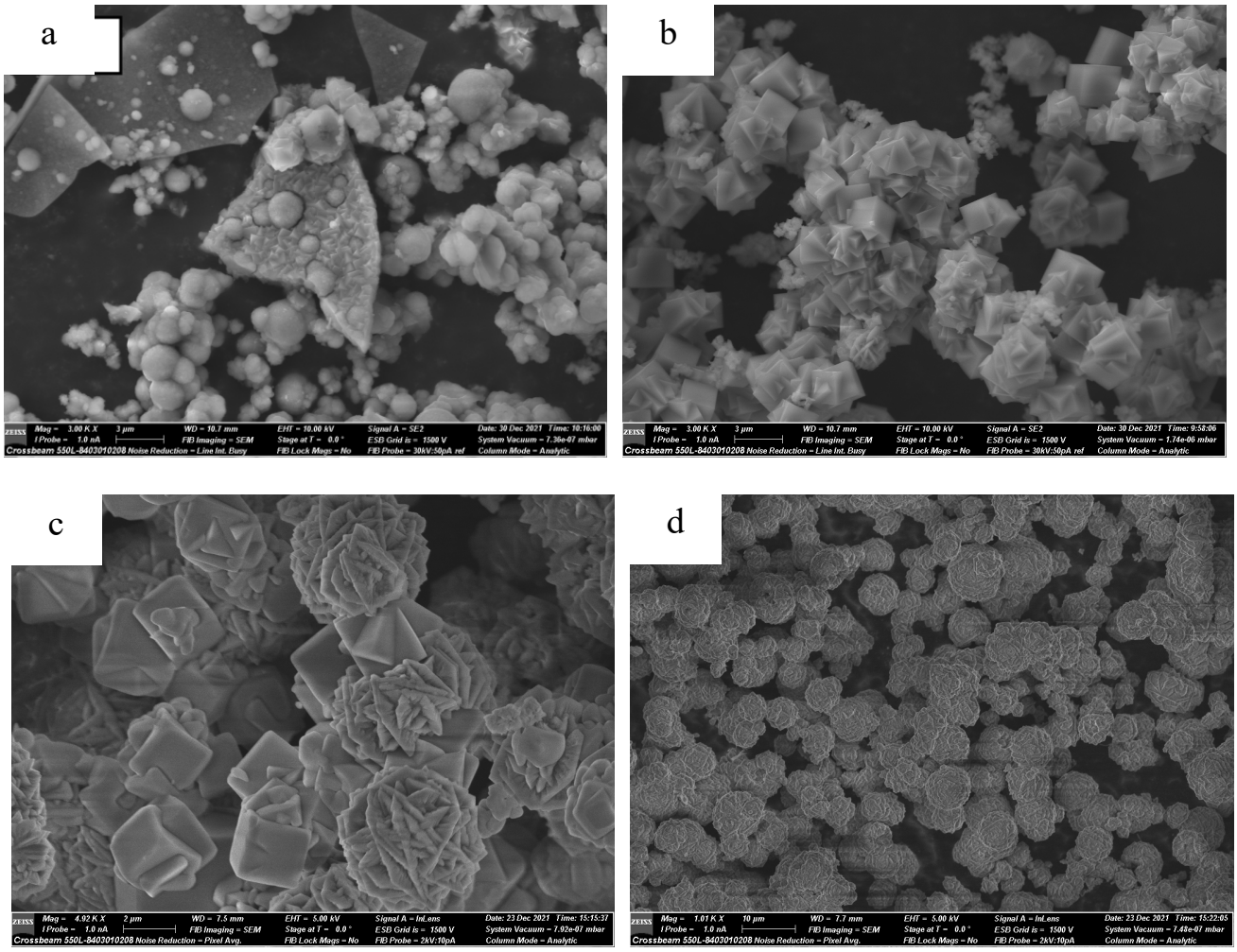


Figure 5. SEM images of zeolites synthesized at different crystallization times. (**a**) Refers to the solid substance naturally precipitated at an ambient temperature; (**b**) refers to the crystallization product for 1 h; (**c**) refers to the crystallization product for 3 h; (**d**) refers to the crystallization product for 5 h.

3.4. REEs Extraction of the Solid Residue via the Acid Leaching

After the CFA was activated and washed, the REEs that originally occurred in the silicate aluminate bonded state in CFA can be released. REEs became their oxides through the calcination treatment and accessible through the water and alkali washing treatment, which was likely to be easily soluble in weak acid solution. Based on our previous experimental study, the pH of the leaching solution at about 2.00 could leach-out REE oxides efficiently, following the leaching reaction equation in the acid leaching condition as follows:

$$Re_2O_3 + 6H^+ \rightleftharpoons 2Re^{3+} + 3H_2O \quad (6)$$

Figure 6a,b show the extraction efficiency results of the single element of LREEs and HREEs, while Table 6 shows those of the total LREEs, the total HREEs, the total REEs as well as the acid consumption. In Figure 6 and Table 6, Treatment 1 represents the acid leaching of the activated CFA sample without further water and alkali washing treatment, Treatment 2 represents the acid leaching of the activated CFA sample with only the water washing, Treatment 3 represents the acid leaching of the activated CFA after both water and alkali washing. In Treatment 1, the extraction efficiency of the total REEs could be achieved by 88.81%. Among them, the extraction efficiency of HREEs and LREEs reached 100.63% and 84.07%, respectively, and only Ce and Tb were somehow lower at only 68.35% and 50.48%, respectively. This is likely due to the transition of some Tb^{3+} to Tb^{4+} in CFA

under an elevated calcination temperature, and the leaching-out of Tb^{4+} was more difficult using hydrochloric acid [42]. In Treatment 2, the extraction efficiency of the total REEs was achieved by 92.23%, among which that of LREEs was slightly improved and that of HREEs was still maintained as very high. Even the extraction efficiency of Ce has been significantly improved, reaching 77.66%. In Treatment 3, the extraction efficiency of the total REEs reached 91.24%, and as expected, the LREEs and HREEs were similarly high.

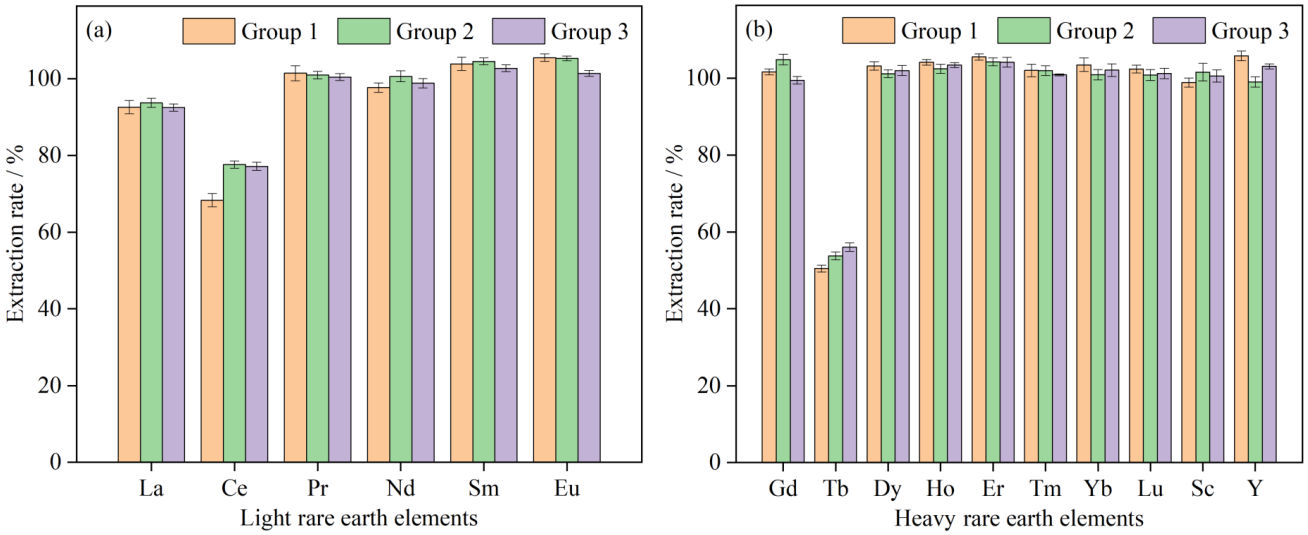


Figure 6. Extraction rate of single REE from CFA with different treatment methods. (**a**) Light rare earth elements (LREEs) and (**b**) Heavy rare earth elements (HREEs). Note: The standard deviations of all REEs extraction rates were less than 2%, and the extraction rate of some REEs exceeds 100%, which is due to the error in the allowable range of trace in the detection of ICP-MS instrument. The content of these REEs is small, which has little impact on the calculation of the extraction rate of total REEs.

Table 6. Hydrochloric acid dosage and extraction rate of LREEs, HREEs, and total REEs corresponding to different treatment methods.

Treatment	Acid Consumption	LREEs	HREEs	SUM
1	3.55 ± 0.02 mL	84.07 ± 0.09%	100.63 ± 1.2%	88.81%
2	2.69 ± 0.03 mL	89.24 ± 0.1%	99.69 ± 0.38%	92.23%
3	0.9 ± 0.04 mL	87.15 ± 0.06%	100.47 ± 0.11%	91.24%

Comparing the three groups and the relevant results in the literature shown in Table 7, one may find a beneficial improvement in the acid leaching of REEs via the treatment of water and alkali washing procedures. The REEs extraction rate has significantly improved. The water and alkali washing jointly worked on the removal of water-soluble Na_2SiO_3 and water-insoluble aluminosilicate in the activated CFA. Therefore, the porous structure was developed to allow the REEs within CFA to be accessible. Moreover, the water and alkali washing could reduce the silica precipitation during the follow-up of acid leaching, resulting in the significant acid saving. This has been clearly shown in Table 6. For the hydrochloric acid consumption among the three groups, the acid consumption was 3.55 $mL \cdot g^{-1}$ in Treatment 1, dropped to 2.69 $mL \cdot g^{-1}$ in Treatment 2, and significantly dropped to 0.9 $mL \cdot g^{-1}$ in Treatment 3, achieving a total of 74.5% in acid saving. It is clear that the Na_2SiO_3 and aluminosilicate remaining in the activated CFA consume a large amount of acid.

Table 7. Comparison with REEs extraction rates in literature.

Sample	Treatment	Extraction Rate
Coal fly ash	85 °C, 6.25 mol/L NaOH alkaline solution, 20% HCl acid leaching	85%
Coal fly ash	350 °C, fly ash and NaOH mixed roasting (1:1), 1–2 mol/L HNO_3 leaching	>70%
Coal fly ash	850 °C, fly ash and Na_2CO_3 mixed roasting (1:1), 3 mol/L HCl leaching	73%
Coal fly ash	150 °C, 40% NaOH alkaline solution, 8 mol/L HCl acid leaching	88.2%
Coal fly ash	This research	91.24%

4. Conclusions

The following conclusions can be drawn from this study:

(1) The activation of CFA was achieved by the Na_2CO_3 calcination effectively at 850 °C for 80 min. The following washing with water and alkali could significantly reduce the silicate aluminate constituents in the activated CFA sample. The REEs contained in the treated solid residue can be easily and successfully extracted while greatly reducing acid consumption during the acid leaching process. The acid saving rate was achieved by 74.5%, and the extraction rate of total REEs was achieved by 91.24%.

(2) The optimal alkali washing conditions of the activated sample were found to be 20% NaOH as the alkali washing solution, 60 °C in temperature, 1:20 in a solid–liquid ratio, and 1 h in holding time. The removal or extraction efficiencies of Al and Si were achieved by 62.51% and 88.28%, respectively.

(3) For the value-added products obtained, the yield of the precipitated silica product was achieved as high as 257.58 g/kg. The generated class A commercial white carbon black single crystal was around 40 nm in its individual grain size, 338.1 m^2/g in its BET surface areas, and more than 93% in its purity. The production of the obtained zeolites, mainly sodalite and class A zeolite, was achieved in a yield of 410.3 g/kg after 5 h of crystallization.

Author Contributions: Conceptualization, Y.C.; data analysis, Y.C. and Z.S.; investigation and methodology, Y.C., Z.S., H.L. and Z.T.; project administration, Y.C.; writing—original draft, Y.C.; visualization, B.W., L.G. and Y.X.; writing—review and editing, all co-authors. All authors have read and agreed to the published version of the manuscript.

Funding: This work was supported by grants from the National Natural Science Foundation of China (Grant No. 22178339), 2023 Innovation-driven Development Special Foundation of Guangxi Province, the University Science Research Project of Anhui Province (No. 2022AH050076), the Hundred Talents Program (A) of the Chinese Academy of Sciences, and the Polygeneration Cycle Coupling Coal-based Hydrogen Production Project of Shanxi Science and Technology Research Institute of Jinneng Holding Group.

Institutional Review Board Statement: Not applicable.

Informed Consent Statement: Not applicable.

Data Availability Statement: The datasets used and/or analyzed during the current study are available from the corresponding author on reasonable request.

Conflicts of Interest: The authors declare no conflict of interest.

References

1. Gao, H.; Huang, Y.; Li, W.; Li, J.; Ouyang, S.; Song, T.; Lv, F.; Zhai, W.; Ma, K. Explanation of heavy metal pollution in coal mines of China from the perspective of coal gangue geochemical characteristics. *Environ. Sci. Pollut. Res.* **2021**, *28*, 65363–65373. [CrossRef]
2. Cao, L.; Appel, E.; Rösler, W.; Magiera, T. Efficiency of stepwise magnetic-chemical site assessment for fly ash derived heavy metal pollution. *Geophys. J. Int.* **2015**, *203*, 767–775. [CrossRef]
3. Sun, Y.-q.; Xiao, K.; Wang, X.-d.; Lv, Z.-h.; Mao, M. Evaluating the distribution and potential ecological risks of heavy metal in coal gangue. *Environ. Sci. Pollut. Res.* **2021**, *28*, 18604–18615. [CrossRef]
4. Dong, Y.-b.; Liu, Y.; Lin, H. Leaching behavior of V, Pb, Cd, Cr, and As from stone coal waste rock with different particle sizes. *Int. J. Miner. Metall. Mater.* **2018**, *25*, 861–870. [CrossRef]

5. Sibanda, V.; Ndlovu, S.; Dombo, G.; Shemi, A.; Rampou, M. Towards the utilization of fly ash as a feedstock for smelter grade alumina production: A review of the developments. *J. Sustain. Metall.* **2016**, *2*, 167–184. [CrossRef]
6. Mahedi, M.; Cetin, B.; White, D. Cement, lime, and fly ashes in stabilizing expansive soils: Performance evaluation and comparison. *J. Mater. Civ. Eng.* **2020**, *32*, 04020177. [CrossRef]
7. Chandan Kumar, D.; Vasanthi, P.; Devaraju, A. Experimental studies on composite bricks using black cotton soil, fly ash and granite waste. *Mater. Today Proc.* **2021**, *39*, 868–874. [CrossRef]
8. Mi, H.; Yi, L.; Wu, Q.; Xia, J.; Zhang, B. Preparation of high-strength ceramsite from red mud, fly ash, and bentonite. *Ceram. Int.* **2021**, *47*, 18218–18229. [CrossRef]
9. Kan, L.-l.; Wang, W.-s.; Liu, W.-d.; Wu, M. Development and characterization of fly ash based PVA fiber reinforced engineered geopolymer composites incorporating metakaolin. *Cem. Concr. Compos.* **2020**, *108*, 103521. [CrossRef]
10. Gollakota, A.R.K.; Volli, V.; Shu, C.-M. Progressive utilisation prospects of coal fly ash: A review. *Sci. Total Environ.* **2019**, *672*, 951–989. [CrossRef]
11. Yao, Z.T.; Ji, X.S.; Sarker, P.K.; Tang, J.H.; Ge, L.Q.; Xia, M.S.; Xi, Y.Q. A comprehensive review on the applications of coal fly ash. *Earth-Sci. Rev.* **2015**, *141*, 105–121. [CrossRef]
12. Yoldi, M.; Fuentes-Ordoñez, E.G.; Korili, S.A.; Gil, A. Zeolite synthesis from industrial wastes. *Microporous Mesoporous Mater.* **2019**, *287*, 183–191. [CrossRef]
13. Zhao, S.; Wen, Q.; Zhang, X.; Liu, B.; Zhang, S. Migration, transformation and solidification/stabilization mechanisms of heavy metals in glass-ceramics made from MSWI fly ash and pickling sludge. *Ceram. Int.* **2021**, *47*, 21599–21609. [CrossRef]
14. Dutta, T.; Kim, K.-H.; Uchimiya, M.; Kwon, E.E.; Jeon, B.-H.; Deep, A.; Yun, S.-T. Global demand for rare earth resources and strategies for green mining. *Environ. Res.* **2016**, *150*, 182–190. [CrossRef]
15. Dai, S.; Finkelman, R.B. Coal as a promising source of critical elements: Progress and future prospects. *Int. J. Coal Geol.* **2018**, *186*, 155–164. [CrossRef]
16. Salem, M.; Souissi, R.; Souissi, F.; Abbes, N.; Moutte, J. Phosphoric acid purification sludge: Potential in heavy metals and rare earth elements. *Waste Manag.* **2019**, *83*, 46–56. [CrossRef] [PubMed]
17. Zhang, W.; Yang, X.; Honaker, R.Q. Association characteristic study and preliminary recovery investigation of rare earth elements from Fire Clay seam coal middlings. *Fuel* **2018**, *215*, 551–560. [CrossRef]
18. Wu, D.; Feng, J.; Chu, S.; Jacobs, D.F.; Tong, X.; Zhao, Q.; Chen, X.; Zeng, S. Integrated application of sewage sludge, earthworms and Jatropha curcas on abandoned rare-earth mine land soil. *Chemosphere* **2019**, *214*, 47–54. [CrossRef] [PubMed]
19. Soyol-Erdene, T.O.; Valente, T.; Grande, J.A.; de la Torre, M.L. Mineralogical controls on mobility of rare earth elements in acid mine drainage environments. *Chemosphere* **2018**, *205*, 317–327. [CrossRef]
20. Stoy, L.; Diaz, V.; Huang, C.-H. Preferential recovery of rare-earth elements from coal fly ash using a recyclable Ionic liquid. *Environ. Sci. Technol.* **2021**, *55*, 9209–9220. [CrossRef]
21. Dai, S.; Zhao, L.; Hower, J.C.; Johnston, M.N.; Song, W.; Wang, P.; Zhang, S. Petrology, mineralogy, and chemistry of size-fractioned fly ash from the Jungar power plant, Inner Mongolia, China, with emphasis on the distribution of rare earth elements. *Energy Fuels* **2014**, *28*, 1502–1514. [CrossRef]
22. Franus, W.; Wiatros-Motyka, M.M.; Wdowin, M. Coal fly ash as a resource for rare earth elements. *Environ. Sci. Pollut. Res.* **2015**, *22*, 9464–9474. [CrossRef] [PubMed]
23. Zhang, W.; Rezaee, M.; Bhagavatula, A.; Li, Y.; Groppo, J.; Honaker, R. A review of the occurrence and promising recovery methods of rare earth elements from coal and coal by-products. *Int. J. Coal Prep. Util.* **2015**, *35*, 150708213531007. [CrossRef]
24. Wen, Z.; Zhou, C.-C.; Pan, J.; Cao, S.; Hu, T.; Ji, W.; Nie, T. Recovery of rare-earth elements from coal fly ash via enhanced leaching. *Int. J. Coal Prep. Util.* **2020**, *42*, 2041–2055. [CrossRef]
25. Tang, M.; Zhou, C.-C.; Zhang, N.; Pan, J.; Cao, S.; Hu, T.; Ji, W.; Wen, Z.; Nie, T. Extraction of rare earth elements from coal fly ash by alkali fusion–acid leaching: Mechanism analysis. *Int. J. Coal Prep. Util.* **2019**, *42*, 536–555. [CrossRef]
26. Pan, J.; Hassas, B.V.; Rezaee, M.; Zhou, C.; Pisupati, S.V. Recovery of rare earth elements from coal fly ash through sequential chemical roasting, water leaching, and acid leaching processes. *J. Clean. Prod.* **2021**, *284*, 124725. [CrossRef]
27. Trinh, H.B.; Kim, S.; Lee, J. Recovery of rare earth elements from coal fly ash using enrichment by sodium hydroxide leaching and dissolution by hydrochloric acid. *Geosystem Eng.* **2022**, *25*, 53–62. [CrossRef]
28. Qi, L.; Ji, B.; Xiao, Z.; Zhang, W. Alkali pretreatment effects on acid leaching recovery of rare earth elements from coal waste of the Western Kentucky No. 13 and Fire Clay seams. *Miner. Miner. Mater.* **2022**, *1*, 7. [CrossRef]
29. Shoppert, A.; Valeev, D.; Napol'skikh, J.; Loginova, I.; Pan, J.; Chen, H.; Zhang, L. Rare-Earth Elements Extraction from Low-Alkali Desilicated Coal Fly Ash by $(NH_4)_2SO_4$+H_2SO_4. *Materials* **2022**, *16*, 6. [CrossRef]
30. Shoppert, A.; Loginova, I.; Valeev, D. Kinetics Study of Al Extraction from Desilicated Coal Fly Ash by NaOH at Atmospheric Pressure. *Materials* **2021**, *14*, 7700. [CrossRef]
31. Li Ruiqing, W.Y. Extraction of Rare Earth Elements from Waste Rare Earth Tribasic Fluorescent Powder by High Temperature Alkali Melting Method. In Proceedings of the 2012 International Symposium on Metallurgy and Materials Analysis and Testing, Beijing, China, 29 October–3 November 2012.
32. Haiyong, N. A Method for Recycling Rare Earth Elements from Waste Fluorescent Lamps. CN101307391, 19 November 2008.
33. Huang, C.; Wang, Y.; Huang, B.; Dong, Y.; Sun, X. The recovery of rare earth elements from coal combustion products by ionic liquids. *Miner. Eng.* **2019**, *130*, 142–147. [CrossRef]

34. Zhang, J.-B.; Li, S.-P.; Li, H.-Q.; He, M.-M. Acid activation for pre-desilicated high-alumina fly ash. *Fuel Process. Technol.* **2016**, *151*, 64–71. [CrossRef]
35. Chen, Y.; Liu, P.; Yu, Z.; Tan, J. Synthesis of nanosized NaY molecular sieve under dynamic hydrothermal crystallization. *Key Eng. Mater.* **2014**, *609–610*, 288–297. [CrossRef]
36. Quang, D.V.; Sarawade, P.B.; Hilonga, A.; Park, S.D.; Kim, J.-K.; Kim, H.T. Facile route for preparation of silver nanoparticle-coated precipitated silica. *Appl. Surf. Sci.* **2011**, *257*, 4250–4256. [CrossRef]
37. El-Sakhawy, M.; Adel, A.M.; Diab, M.A.; Al-Shemy, M. Facile methods for the preparation of micro- and mesoporous amorphous silica from rice husk. *Biomass Convers. Biorefinery* **2022**, *12*, 4709–4718. [CrossRef]
38. Ijaz, A.; Yagci, M.B.; Ow-Yang, C.W.; Demirel, A.L.; Mikó, A. Formation of mesoporous silica particles with hierarchical morphology. *Microporous Mesoporous Mater.* **2020**, *303*, 110240. [CrossRef]
39. Zhang, J.; Lu, P.; Teng, Y.; Wang, S.; Zhang, L. In-situ surface modification of precipitated silica nanoparticles with 3-methacryloxypropyltrimethoxysilane in carbonation process. *Res. Chem. Intermed.* **2021**, *47*, 3037–3050. [CrossRef]
40. Greer, H.; Wheatley, P.S.; Ashbrook, S.E.; Morris, R.E.; Zhou, W. Early Stage Reversed Crystal Growth of Zeolite A and Its Phase Transformation to Sodalite. *J. Am. Chem. Soc.* **2009**, *131*, 17986–17992. [CrossRef] [PubMed]
41. Subotić, B.; Škrtić, D.; Šmit, I.; Sekovanić, L. Transformation of zeolite A into hydroxysodalite: I. An approach to the mechanism of transformation and its experimental evaluation. *J. Cryst. Growth* **1980**, *50*, 498–508. [CrossRef]
42. Wu, W. *Rare Earth Metallurgy*; Chemical Industry Press (CIP): Beijing, China, 2005; Volume 8, pp. 2–7.

Disclaimer/Publisher's Note: The statements, opinions and data contained in all publications are solely those of the individual author(s) and contributor(s) and not of MDPI and/or the editor(s). MDPI and/or the editor(s) disclaim responsibility for any injury to people or property resulting from any ideas, methods, instructions or products referred to in the content.